Emission characteristics of water in the Universe

Poelman, Dieter Roel

Chapter 4

The interpretation of water emission from dense interstellar clouds

Existing SWAS observations and future HIFI/Herschel data require a clear sense of the information content of water emission and absorption lines. We investigate whether the ground-state transition of ortho-H_2O (1_{10}-1_{01}) at 557 GHz can be used to measure the column density throughout an interstellar cloud. We find that for low abundances, i.e., $X(H_2O) \lesssim 10^{-9}$, the intensity of the 1_{10}-1_{01} transition scales with the total column density of H_2. However, this relationship breaks down with increasing abundance, i.e., optical depth, due to line trapping and – for $T_{\rm dust} \gtrsim 25$ K, $X(H_2O) \lesssim 10^{-8}$ and $n \sim 10^4$ cm^{-3} – absorption of the dust continuum. We conclude that an observed decline in intensity per column density, expected if H_2O is a surface tracer, does not necessarily mean that the water is absent in the gas-phase at large column densities, but can be caused by line trapping and subsequent collisional de-excitation. Consequently, to determine the amount of water vapour in the interstellar medium, multiple line measurements of optically thin transitions are needed to disentangle radiative transfer and local excitation effects.

Based on Poelman, D. R., Spaans, M., & Tielens, A. G. G. M. 2007, A&A, 464 1023-1027

4.1 Introduction

The launch of the *Submillimeter Wave Astronomy Satellite* (SWAS, Melnick et al. 2000) made it possible to observe emission from the ground-state transition (1_{10}-1_{01}) of ortho-$H_2^{16}O$ and its isotopomer ortho-$H_2^{18}O$, to determine the abundance of water vapour, i.e., column density $N_{\text{o-}H_2O}$, in various regions in the interstellar medium, e.g., dense and diffuse interstellar gas clouds, circumstellar envelopes, planetary atmospheres, and comets (e.g., Melnick et al. 2000; Snell et al. 2000a,b; Encrenaz et al. 1995; Bergin et al. 2000a; Gurwell et al. 2000; Melnick et al. 2000). In the future, the *Heterodyne Instrument for the Far Infrared* (HIFI) on *Herschel* will observe even more transitions of ortho- and para-H_2O (o/p-H_2O) like 2_{12}-1_{01} (1669.904 GHz), 2_{21}-2_{12} (1661.015 GHz), 3_{03}-2_{12} (1716.774 GHz), 3_{12}-3_{03} (1097.357 GHz), 3_{21}-3_{12} (1162.910 GHz), 1_{11}-0_{00} (1113.342 GHz), 2_{02}-1_{11} (967.924 GHz), 2_{11}-2_{02} (752.029 GHz), and 2_{20}-2_{11} (1228.801 GHz), with some in absorption while others in emission.

One of the main goals of the SWAS mission was to determine where and whether H_2O and O_2 are the major reservoirs of oxygen through the interstellar medium. SWAS observations have determined the gaseous water abundance in warm dense gas ($T \gtrsim 300$ K and $n(H_2) \gtrsim 10^3$ cm^{-3}) to be 10^{-5} relative to H_2, in good agreement with chemical models for such conditions. However, in cold ($T \lesssim 30$ K), dense clouds the abundance of gaseous water is ~ 100 to 1000 times below the predictions of cold-cloud gas-phase chemical models. It has been suggested that toward cold clouds gaseous H_2O exists only near the cloud surface. Indeed, closer to the surface than an A_V of a few mag, H_2O is photodissociated by the ambient galactic UV field. Deeper into the cloud, i.e., A_V of $4-8$ mag (depending on density and UV intensity), H_2O may rapidly deplete onto dust grains (Bergin et al. 2000b; Charnley et al. 2001; Viti et al. 2001). Although the derivation of the column density from absorption observations is straightforward (column density is simply proportional to the optical depth in the line, see Plume et al. 2004), this is not the case for emission observations. The analysis to determine the H_2O abundance now crucially depends on the physical properties of the gas through the collisional rate coefficients. Therefore, accurate constraints on the gas densities and temperatures are needed.

Extensive SWAS observations of the Orion A molecular cloud show that gaseous H_2O correlates with CN rather than with $C^{18}O$ (Melnick & Bergin 2005, see Fig. 4.1). From model calculations (e.g., Sternberg & Dalgarno 1995; Jansen et al. 1995) we know that in homogeneous photon dominated regions (PDRs) CN molecules, just as HCO^+, are abundant in zones closer to the PDR surface where the ultraviolet (UV) radiation field is only partly attenuated, whereas CO is more a volume tracer (Fig. 4.1). Because of this behaviour, the observational correlation of H_2O with CN has been interpreted as evidence that gaseous water resides only near the sur-

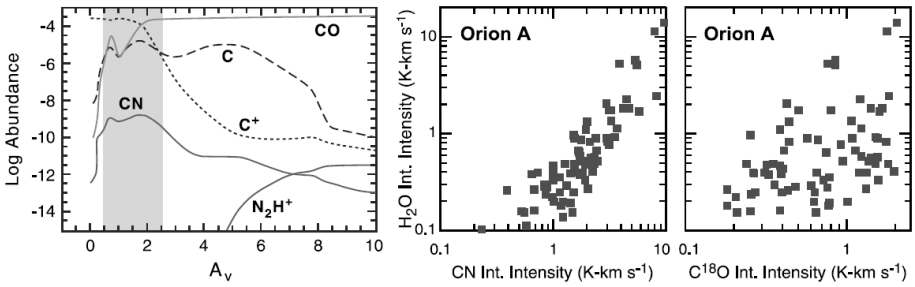

Figure 4.1: (*Left*) Predicted CN, CO, C, C^+ and N_2H^+ abundance versus depth into the cloud with $n(\mathrm{H}) = 10^6\ \mathrm{cm}^{-3}$, $G_0 = 2 \times 10^5$, and a cosmic-ray ionization rate $\zeta = 5 \times 10^{-17}\ \mathrm{s}^{-1}$ (after Sternberg and Dalgarno, 1995). The shaded region highlights the depths, near to the cloud surface, where the CN abundance is predicted to peak. CO is a volume tracer. (*Middle*) H_2O (1_{10}-1_{01}) versus CN (J = 1-0) integrated intensity towards the ridge in Orion A. (*Right*) H_2O (1_{10}-1_{01}) versus $C^{18}O$ (J = 1-0) integrated intensity toward the same lines of sight. The H_2O data were obtained with SWAS. Both the CN and $C^{18}O$ data were obtained with FCRAO telescope and the spatial resolution was convolved to match that of SWAS (Melnick & Bergin 2005).

face. However, caution is needed when relying purely on single transition observations to draw such a conclusion in view of the complex rotational level structure of the H_2O molecule. In particular, there is a fundamental difference between an optically thin and an effectively optically thin line. The latter case implies a strong coupling between line photons and water molecules. A full radiative transfer calculation is needed to address this problem, since the observed intensities of molecular emission depend on a complex competition between radiative and collisional processes. Moreover, the excitation of H_2O differs from that of other molecules, since both collisions and infrared radiation from warm dust influence the level populations (Takahashi et al. 1983). The intent of this work is to show that it is not a straightforward matter to retrieve accurate information, e.g., column density, from single transition observations of H_2O due to the complex level structure of this molecule.

4.2 Model description and results

We calculate the surface brightness for the 1_{10}-1_{01} ground-state transition of o-H_2O, in the case of a homogeneous sphere and as a function of impact parameter. The density and abundance of H_2O are the main parameters of the model. All the models have a constant total column density $N(H_2)$ of $6 \times 10^{21}\ \mathrm{cm}^{-2}$ through the center of the cloud, corresponding to a total A_V of

Table 4.1: Model parameters

Model	$n(H_2)$ [cm^{-3}]	size [pc]	$X(H_2O)$[a]	$N(H_2)$[b] [cm^{-2}]	T_{gas} [K]	T_{dust} [K]
I	10^4-10^6	0.002–0.2	$10^{-10}-10^{-6}$	6×10^{21}	50	no
II	10^4-10^6	0.002–0.2	$10^{-10}-10^{-6}$	6×10^{21}	50	15
III	10^4-10^6	0.002–0.2	$10^{-10}-10^{-6}$	6×10^{21}	50	25
IV	10^4-10^6	0.002–0.2	$10^{-10}-10^{-6}$	6×10^{21}	50	50
V	10^4-10^6	0.002–0.2	$10^{-10}-10^{-6}$	6×10^{21}	30	15

[a] Abundance of H_2O; [b] Column density through the center

~ 3 mag. As a result, the physical size of the cloud is inversely proportional to the density of the medium. The parameters for the different models are shown in Table 4.1. The density ranges from 10^4 to $10^6\,cm^{-3}$, thereby covering the relevant range for dense molecular clouds such as the Orion ridge. The temperatures, ranging from 30 K to 50 K for the gas and from 15 to 50 K for the dust, were chosen to represent the mean observed temperatures towards star-forming molecular clouds such as the Orion ridge, which were the focus of the SWAS effort. In model I we ignore the emission from dust and CMB, whereas a dust temperature between 15 K and 50 K is assumed in models II – IV, in order to assess the influence of the dust and temperature, respectively, on the excitation of the water molecule. The temperatures in model V are a factor of ~ 2 lower than in the other models since, to maintain a temperature of the gas of 50 K throughout the cloud, a strong UV radiation field is needed, which is not always the case. Note that the gas and dust temperatures are independent of cloud depth. The intent of this chapter is to illustrate the excitation and radiative transfer effects assuming a 'simple' cloud model, not to model a realistic cloud. A Galactic dust-to-gas ratio of 10^{-2} by mass is assumed. In all the models except for model I, the dust optical depth τ_{dust} through the center of the cloud at the frequency of the ground-state transition of o-H_2O is 10^{-3}. Within each model the water abundance $X(H_2O)$ ranges from 10^{-10} to 10^{-6}. Throughout the models, a velocity dispersion of $1\,km\,s^{-1}$ is adopted, as is typical of a cloud with moderate turbulence. Note that the results presented in this chapter depend on the adopted velocity dispersion. A higher (lower) velocity dispersion will decrease (increase) the optical depth for a given transition, thereby having an impact on the excitation of the molecule.

Figures 4.2 – 4.4 present the basic results of this work. We plot, as a function of $N(H_2)$, i.e., different impact parameter, the 1_{10}-1_{01} line intensity above the continuum per unit column density of o-H_2O. The results for model I, in which we ignore the contribution of dust and CMB on the excitation of the water molecule are displayed in Fig. 4.2. The position of the $\tau = 1$ surface is denoted by a cross for $X(H_2O) = 10^{-9}$–10^{-6}. Models II, III, and IV

behave in a similar way as in model I in the case $n(H_2) \geq 10^5$ cm^{-3}. For this reason, we only plot the outcome in the low density case for models II, III, and IV in Fig. 4.3. The results for model V are plotted in Fig. 4.4.

The following trends can be identified, which will be discussed in Sect. 4.3. First, in the case of $n(H_2) \geq 10^5$ cm^{-3} and $X(H_2O) \lesssim 10^{-8}$, i.e., $\tau < 10$, a linear relationship holds between the number of photons escaping the cloud and the impact parameter, i.e., I/N_{H_2O} is constant. However, this relationship breaks down at a high optical depth, i.e., $H_2O > 10^{-8}$, for all the models. Second, in all the models except model I, absorption occurs in the low density case when abundances are low, i.e., $X(H_2O) < 10^{-8}$, which becomes more apparent as the dust temperature increases. However, the amount of absorption is moderate as the self-reversal in the center of the line is small. Third, when the H_2O abundance exceeds 10^{-7}, the ratio of the intensity to the column density decreases near the edge of the cloud ($N(H_2) \sim 5 \times 10^{20}$ cm^{-2}) in all the models. Fourth, for high optical depth, i.e., $X(H_2O) \gtrsim 10^{-7}$ and $n(H_2) = 10^6$ cm^{-3}, I/N_{H_2O} decreases with increasing column density. Fifth, lowering the gas and dust temperatures by a factor of ~ 2 (model V) does not lead to significant differences in the shapes of the curves. That is, models II – IV and model V experience similar complicating radiative transfer effects.

4.3 Discussion

The asymmetry of the water molecule causes the rotational levels to split into a number of different ladders, so called 'K-ladders', characterized by different values of the projection of the angular momentum onto the principal axes of the molecule ($J_{K_aK_c}$), as discussed in Chapter 1. Radiative transitions occur rapidly between levels in each ladder but are much slower between levels in different ladders. This leads to a more complex spectrum than linear or symmetric top molecules, e.g., CO, NH_3. Hence, disentangling the different processes that contribute to the observed spectrum is not straightforward. We now describe the different effects that play a role in interpreting the figures. In this, the 'edge' and 'center' of the cloud refers to an impact parameter of 1 and 0, respectively. Note that the use of spherical models leads to angular non-trivial re-distribution of line photons. The same holds for continuum photons within the line-profile frequency range.

First, one can see in Figs. 4.2 and 4.4 that the curves as function of total column density (H_2) are constant for $X(H_2O) \lesssim 10^{-8}$ and $n(H_2) \geq 10^5$ cm^{-3}. In this limit, collisional de-excitation and scattering effects are negligible. Eventually every photon produced in the cloud will escape the cloud with few interactions with the surrounding medium. Note that the number of scatterings N to escape depends on the optical depth. Therefore, in the regime $\tau \ll 1$ few photons are scattered and $N \approx \tau$. With increasing optical

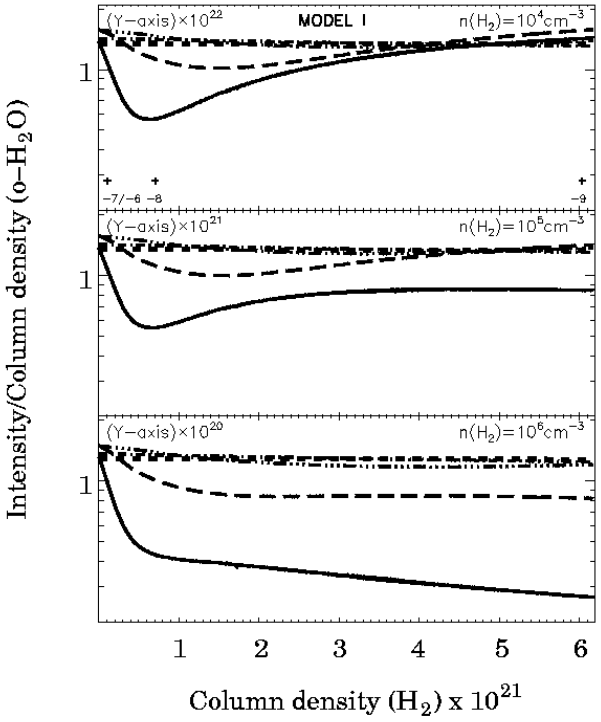

Figure 4.2: The intensity of the ortho-H_2O ground-state transition for a homogeneous sphere with H_2 densities of 10^4 (*top*), 10^5 (*middle*), 10^6 (*bottom*) cm^{-3} and temperature of the gas of 50 K. The dust emission, as well as the CMB radiation, is ignored (i.e., model I). In every case, the total column density (H_2) is kept constant. Lines are plotted for an abundance of H_2O, relative to H_2, of 10^{-10} (*dashed*), 10^{-9} (*dash dot*), 10^{-8} (*dash dot dot*), 10^{-7} (*long dashes*), and 10^{-6} (*solid*) as a function of H_2 column density along the line of sight, where 2×10^{19} cm^{-2} is at the edge, and 6×10^{21} cm^{-2} is through the center of the cloud. The Y-axis is in units of erg s^{-1}sr^{-1}. The position of the $\tau=1$ surface is displayed with a cross for $X(H_2O)=10^{-9}$–10^{-6}.

depth, i.e., $X(H_2O)\gtrsim10^{-8}$, more effects need to be taken into account. All models show a drop near the edge of the cloud. Because of the increasing optical depth, line-scattering effects become important. Thus, line photons then tend to escape in the direction with the lowest optical depth rather than tangentially to the cloud surface, causing the dip near the edge. However, towards the center of the cloud, the optical depth increases with orders of magnitude. The photons will undergo numerous scatterings for $\tau\gg1$, with $N\approx\tau^2$, and eventually will escape in the line wings.

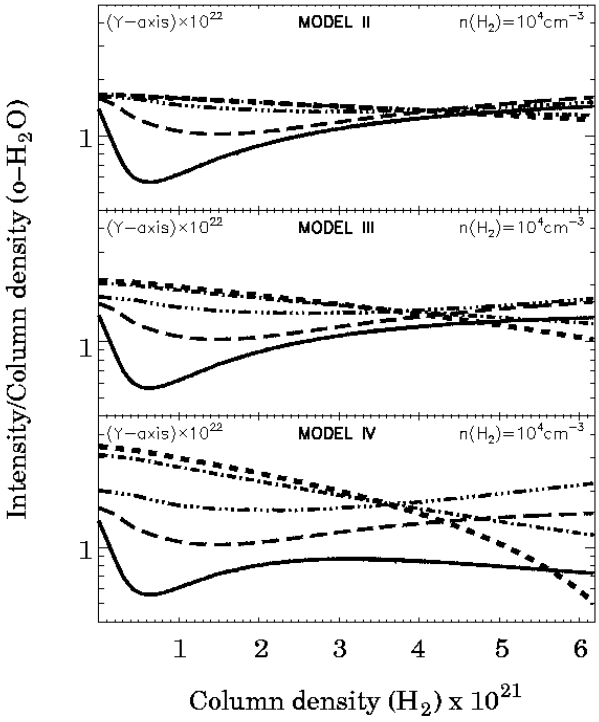

Figure 4.3: The intensity of the ortho-H_2O ground-state transition for a homogeneous sphere with density (H_2) of 10^4 cm^{-3} for model II (*top*), III (*middle*), and IV (*bottom*). Lines are plotted for an abundance of H_2O, relative to H_2, of 10^{-10} (*dashed*), 10^{-9} (*dash dot*), 10^{-8} (*dash dot dot*), 10^{-7} (*long dashes*), and 10^{-6} (*solid*) as a function of H_2 column density along the line of sight, where 2×10^{19} cm^{-2} is at the edge, and 6×10^{21} cm^{-2} is through the center of the cloud. The Y-axis is in units of erg s^{-1} sr^{-1}.

Second, at densities as low as 10^4 cm^{-3} and abundances not exceeding 10^{-8} (modest optical depth) the line is strongly subthermally excited and radiatively colder than the dust background. Hence, the line appears in absorption. The decrease in $I/N(H_2O)$ shown in Fig. 4.3 now indicates that lines of sight through the cloud center are no longer contributing evenly to the emissivity across their entire column. The line is not strictly in absorption yet, but it has developed an intensity dip around line center. Thus, the presence of dust causes the trend in the intensity per column density in this regime to decrease (Takahashi et al. 1983). This behaviour is not seen in case $n(H_2)\gtrsim10^5$ cm^{-3}, as collisions are the dominant process in the exci-

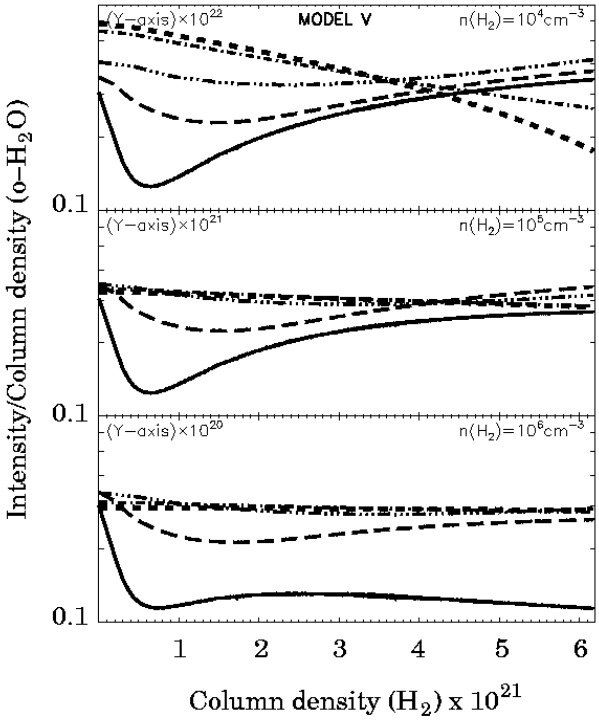

Figure 4.4: The intensity of the ortho-H_2O ground-state transition in case of a homogeneous sphere with densities (H_2) of 10^4 (*top*), 10^5 (*middle*), 10^6 (*bottom*) cm^{-3} and temperatures for gas and dust of 30 K and 15 K, respectively (i.e., model V). In every case, the total column density (H_2) is kept constant. Lines are plotted for an abundance of H_2O, relative to H_2, of 10^{-10} (*dashed*), 10^{-9} (*dash dot*), 10^{-8} (*dash dot dot*), 10^{-7} (*long dashes*), and 10^{-6} (*solid*) as a function of H_2 column density along the line of sight, where 2×10^{19} cm^{-2} is at the edge, and 6×10^{21} cm^{-2} is through the center of the cloud. The Y-axis is in units of erg s^{-1} sr^{-1}.

tation of the water molecule in this regime, thereby nullifying the effect of dust emission. The influence of dust on the excitation/level populations of water is plotted in Fig. 4.5 where the relative population of the 1_{10} level is displayed. One notices that level 1_{10} is more populated for warmer dust. In essence, dust continuum emission will tend to drive the level populations towards a Boltzmann distribution at the temperature of the dust. For a given density, the effects of radiative excitation by dust continuum emission is more pronounced for higher dust temperatures, e.g., higher continuum intensities.

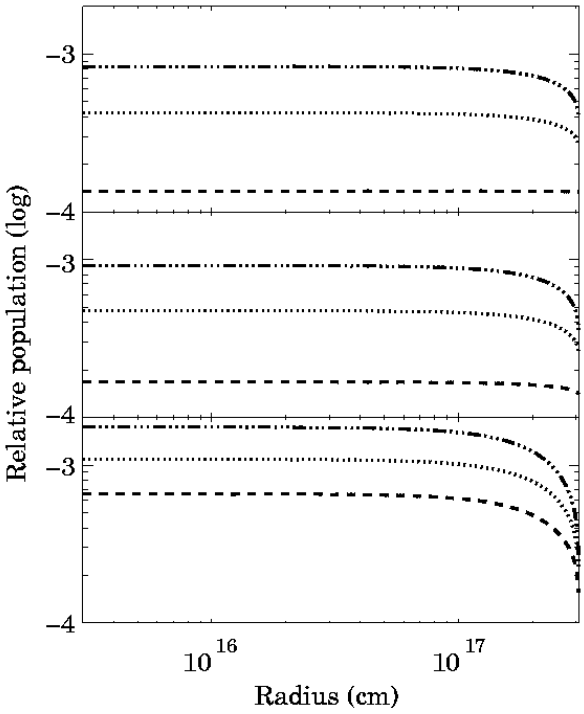

Figure 4.5: The population of the 1_{10} level of ortho-H_2O as function of radius. The top, middle, and bottom panels are the results in case $X(H_2O) = 10^{-10}$, 10^{-9}, 10^{-8}, respectively. Dashed, dotted, and dash-dotted lines represent the results of model I, III, and IV, respectively.

Third, the effect of photon trapping is to lower the density at which local thermodynamic equilibrium (LTE) is approached, i.e., after each absorption, the gas has a chance to collisionally de-excite the species and return the excitation energy to the thermal bath of the gas. For optically thin gas, the critical density of the ground-state transition at 557 GHz of o-H_2O is $\sim 10^8$ cm^{-3} at 50 K. The optical depth through the center of the cloud varies from 0.1 to 10^3 when the abundance rises between 10^{-10} to 10^{-6} in all the models. Hence, for high abundances, i.e., $X(H_2O) \gtrsim 10^{-7}$, the effective critical density drops to 10^5–10^6 cm^{-3}, since $\beta(\tau) \sim 1/\tau$ for high optical depths. Collisional de-excitation processes then become important in the regime where $n(H_2) \gtrsim 10^5$ cm^{-3} and $X(H_2O) \gtrsim 10^{-7}$. It is seen in Figs. 4.2 and 4.4 that the I/N_{H_2O} drops as function of impact parameter for $n(H_2) = 10^6$ cm^{-3} and $X(H_2O) = 10^{-6}$. In this part of parameter space, collisional de-excitation

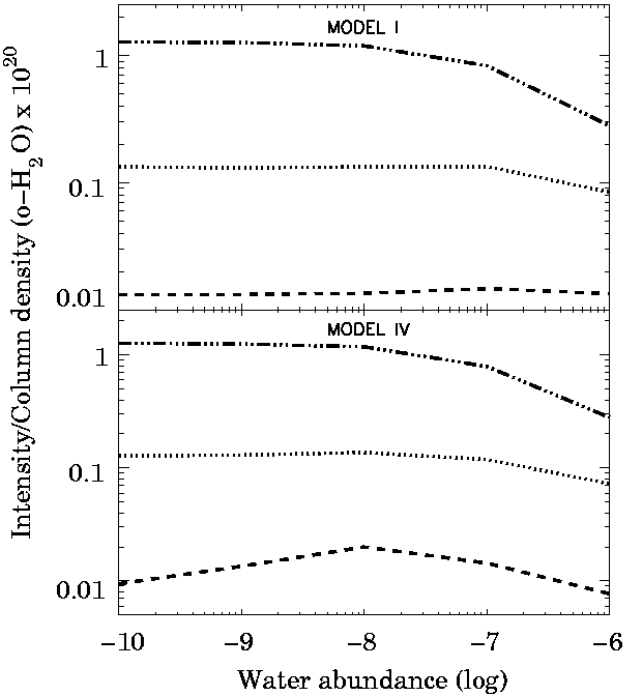

Figure 4.6: Conversion of the results of models I (*top*) and IV (*bottom*) into surface area weighted values. In each panel the dash-dotted, dotted, and dashed curves represent the results in case the density $n(H_2)$ is 10^6, 10^5, and 10^4 cm^{-3}, respectively. The Y-axis is in units of erg s^{-1} sr^{-1}.

is important and the probability is high that line photons are lost to the thermal bath through collisional de-excitation during one of the many scattering events.

Fourth, calculations are performed for model V (Fig. 4.4) with gas temperatures a factor of 2 lower than the temperatures used in model II. We find that the shape of the curves are not affected by such a change in gas temperature. However, it affects the distribution of the level populations and thus the absolute intensity in the lines. Hence, temperature variations cannot dispense with the radiative transfer effects studied in this work.

To summarize, we plot in Fig. 4.6, as a function of abundance, the average intensity emanating from the cloud for models I and IV, i.e.,

$$\frac{\int I_{1_{10}\rightarrow 1_{01}}(b) 2\pi b \, \mathrm{d}b}{\int N_{\mathrm{H_2O}}(b) 2\pi b \, \mathrm{d}b}, \tag{4.1}$$

with b the impact parameter. One notices a drop by a factor of $\sim 2-5$ in the case $n(H_2)$ is $10^5 - 10^6$ cm^{-3}, respectively. Note that with the assumption of an effectively optically thin line one would underestimate the water column density by these same factors.

In addition, models were run with a fixed total column density $N(H_2)$ of 4×10^{22} cm^{-2}, corresponding to an A_V of ~ 20 mag. We find that under the same conditions a maximum drop by a factor $\sim 4-18$ is found in case $n(H_2)$ is $10^5 - 10^6$ cm^{-3}, respectively.

4.4 Astrophysical implications

The intensity of the ground-state transition of o-H_2O is driven by a combination of the ambient gas and dust temperatures on the one side and by the density of the surrounding medium on the other. It is this interplay, together with the complex structure of the molecule, that drives the level populations. To interpret existing SWAS and future HIFI data, a clear picture of the information content of the water lines is needed.

SWAS observations of the lowest rotational transition of o-$H_2^{16}O$ of the Orion A molecular cloud show that gaseous water correlates much better with the near surface tracer CN than with the volume tracer $C^{18}O$, as presented in Melnick & Bergin (2005). Through these observations, in which it is assumed that the ground-state transition of o-H_2O is effectively optically thin, one concludes that water is a surface tracer. This is plausible from a chemical point of view in which photodissociation destroys the water molecule near the surface. Farther inwards the cloud the water abundance reaches its equilibrium value through photodesorption of H_2O-ice and photodestruction of H_2O-gas until it freezes-out onto dust grains deeper into the cloud. However, we have shown (see Fig. 4.6) that the effectively optically thin assumption no longer holds for $\tau > 10$ and $n > 10^5$ cm^{-3}. Hence, under these conditions one is limited to observing the '$\tau = 10$' surface and cannot use water to trace the cloud's volume, even when it is present, i.e., not frozen-out (Cernicharo, private communication). Therefore, as CN is a surface tracer and the water intensity originates from a layer of gas with an optical thickness of 1 – depending on local excitation conditions this layer is a surface layer – the CN intensity correlates much better with the H_2O intensity and not with the volume tracer $C^{18}O$. Thus, the anti-correlation of H_2O with $C^{18}O$ is partly due to optical depth effects, and is not neccesarily a result of chemical changes. As a consequence, the presence of water past the $\tau = 1$ surface cannot be ruled out.

We would also like to point out here that the most interesting aspect of the correlation of the water line intensity with the CN line intensity is that both are observed to vary by a factor ~ 100. Theoretically, the CN abundance is expected to scale with density squared (Boger & Sternberg 2005),

indicating the importance of density variations over the Orion molecular cloud. Given the results presented in this chapter, we surmise that these density variations will hamper the interpretation of the water observations.

In order to deduce the total water column along the line of sight, additional information is needed from other – effectively optically thin – lines. These will be observed with future missions such as Herschel/HIFI.

Acknowledgements

We are grateful to Gary Melnick and Ted Bergin for sending an early version of their paper (Melnick & Bergin 2005) and for the use of Figure 4.1. We also thank Floris van der Tak for helpful discussions and suggestions that have improved the paper and the anonymous referee for his/her constructive comments.

References

Bergin, E. A., Lellouch, E., Harwit, M., et al. 2000a, ApJ, 539, L147
Bergin, E. A., Melnick, G. J., Stauffer, J. R., et al. 2000b, ApJ, 539, L129
Boger, G. I., & Sternberg, A. 2005, ApJ, 632, 302
Charnley, S. B., Rodgers, S. D., & Ehrenfreund, P. 2001, A&A, 378, 1024
Encrenaz, T. H., Lellouch, E., Cernicharo, J., et al. 1995, Icarus, 117, 162
Green, S., Maluendes, S., & McLean, A. D. 1993, ApJS, 85, 181
Gurwell, M. A., Bergin, E. A., Melnick, G. J., et al. 2000, ApJ, 539, L143
Jansen, D. J., Spaans, M., Hogerheijde, M. R., & van Dishoeck, E. F. 1995, A&A, 303, 541
Melnick, G. J., Ashby, M. L. N., Plume, R., et al. 2000, ApJ, 539, L87
Melnick, G. J., & Bergin, E. A. 2005, Advances in Space Research, 36, 1027
Mumma, M. J., Weaver, H. A., & Larson, H. P. 1987, A&A, 187, 419
Ossenkopf, V., & Henning, T. 1994, A&A, 291, 943
Phillips, T. R., Maluendes, S., & Green, S. 1996, ApJS, 107, 467
Plume, R., Kaufman, M. J., Neufeld, D. A., et al. 2004, ApJ, 605, 247
Snell, R. L., Howe, J. E., Ashby, M. L. N., et al. 2000a, ApJ, 539, L101
Snell, R. L., Howe, J. E., Ashby, M. L. N., et al. 2000b, ApJ, 539, L93
Sternberg, A., & Dalgarno, A. 1995, ApJS, 99, 565, SD95
Takahashi, T., Silk, J., & Hollenbach, D. J. 1983 ApJ, 275, 145
van der Tak, F., Neufeld, D., Yates, J., et al. 2005, in The Dusty and Molecular Universe: A Prelude to Herschel and ALMA, ed. A. Wilson, 431
Viti, S., Roueff, E., Hartquist, T. W., Pineau des Forêts, G., & Williams, D. A. 2001, A&A, 370, 557